



# Mechanical properties and thermal conductivity of epoxy composites enhanced by h-BN/RGO and mh-BN/GO hybrid filler for microelectronics packaging application

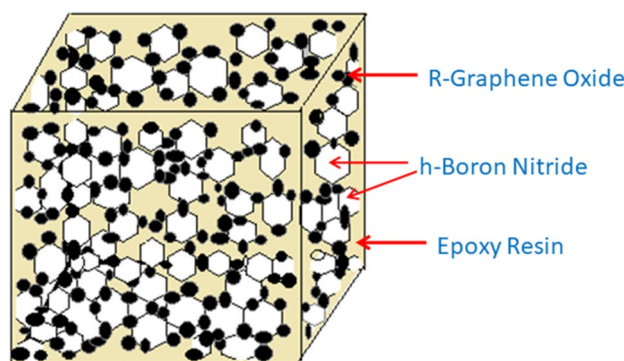
Sagar Kumar Nayak<sup>1</sup> · Smita Mohanty<sup>1</sup> · Sanjay K. Nayak<sup>1,2</sup>

© Springer Nature Switzerland AG 2019

## Abstract

In recent years, significant interest has been focused on fabricating epoxy-based hybrid composite with a high thermal conductivity at optimum filler loading. As epoxy usually has a low thermal conductivity, the high intrinsic thermal conducting fillers such as h-BN, GO and RGO are incorporated. In this research, we report the epoxy-based hybrid composites with an enhanced thermal conductivity through silane-modified h-BN (mh-BN) with RGO. The sample containing 44.5 wt% (40 wt% mh-BN and 4.5 wt% RGO) hybrid filler exhibited the highest thermal conductivity (1.416 W/mK) which was 7 times that of pristine epoxy (0.21 W/mK). The thermal conductivities of RGO with unmodified h-BN (0.789 W/mK), GO with mh-BN (0.769 W/mK) and GO with unmodified h-BN (0.713) at 44.5 wt% loading are also reported. Comparison property studies of these above-mentioned four hybrid composites are described by lap shear strength, flexural strength, impact strength and thermogravimetric analysis. The fabricated hybrid composites exhibit outstanding performance in lap shear strength, thermal stability, and slightly reduced impact and flexural strength, which makes it as relevant for electronics packaging application such semiconductors, integrated circuit packaging, optoelectronics and also can attest potentiality in structural energy storage application. The atomic force microscopy and scanning electron microscopy verified the surface roughness and morphology of two optimized compositions, i.e., mh-BN with RGO and h-BN with RGO with the epoxy matrix. Also, Maxwell, Hashin–Shtrikmann and series equations are used to verify the obtained experimental value.

## Graphical abstract



**Keywords** Epoxy · Graphene oxide (GO) · Reduced graphene oxide (RGO) · Boron nitride (h-BN) · Silane · Thermal conductivity

✉ Sagar Kumar Nayak, email2sagarnayak@gmail.com | <sup>1</sup>Laboratory for Advanced Research in Polymeric Materials (LARPM), Central Institute of Plastics Engineering and Technology (CIPET), B-25, CNI Complex, Patia, Bhubaneswar, Odisha 751024, India. <sup>2</sup>Central Institute of Plastics Engineering and Technology, Chennai, Tamil Nadu 600032, India.

SN Applied Sciences (2019) 1:337 | <https://doi.org/10.1007/s42452-019-0346-2>

Received: 31 December 2018 / Accepted: 7 March 2019 / Published online: 13 March 2019

## 1 Introduction

Due to the rapid advent of the highly efficient integrated circuit, thermal management through thermal interface materials (TIMs) has become a great challenge [1]. Epoxy is well known for its excellent mechanical properties and thermal stability, best adhesion and good electrical insulation properties and compatibility with many materials [2, 3]. Industries need to fabricate high thermal conductivity (TC) and electrically insulative TIMs based on epoxy which is the best option for heat dissipation from electronic circuits to sink. To modify this epoxy (TC ~ 0.21 W/mK) to get required properties, blending of high intrinsic thermal conductive fillers has been incorporated into matrix [3]. The filler includes metal particle such as Cu, Al and Ag, carbon-based filler like graphite plates, CNTs, graphene sheets which are also electrically conductive and ceramic particles like hexagonal boron nitride (h-BN), silicon carbide (SiC), beryllium oxide (BeO), aluminum nitride (AlN), alumina (Al<sub>2</sub>O<sub>3</sub>), which have electrical insulating properties [11]. Among these fillers, graphene oxide (GO) and hexagonal boron nitride (h-BN) hybrid attracts researchers to enhance thermal conductivity with the creation of 3D percolation threshold network inside the matrix which can strain thermal budgets of attached electronic devices [15]. So, this type of hybrid composite is suitable for a wide spectrum of thermal management and electrical application. H-BN is recognized as white graphite, isoelectric with carbon possess, the high intrinsic in-plane thermal conductivity of 30–300 W/mK. Localization of free electron between interlayer of covalent-bonded boron and nitrogen atom makes it electrically insulative [1, 2, 4]. Wang et al. [1] prepared electrical insulating epoxy composite using silane-treated BN nanoplatelets with a maximum TC of 5.24 W/mK. Gu et al. [2] reported that silane-modified BN epoxy resin composites at 60% mass fraction are 1.052 W/mK. Single-layer graphene exhibits high TC (5300 W/mK), and comparable thermal interface resistance of graphene is ~  $3.7 \times 10^{-9}$  m<sup>2</sup>K/W which is marginally lower than CNT ( $8 \times 10^{-8}$  m<sup>2</sup>K/W) [5]. However, 3D network of highly oriented graphene would be used to fabricate high-quality thermal conductive network. GO has been synthesized by modified Hummer's method [6–8]. Park et al. [9] first prepared few-layer graphene (FLG) through interlayer catalytic exfoliation and then incorporated to the epoxy matrix to prepare TIMs demonstrating thermal conductivity of  $3.87 \pm 0.28$  W/mK at 10 vol% of filler loading. Wenhui Yuan et al. prepared heat conducting bridge between GO and a ceramic particle such as AlN as a hybrid filler to incorporate inside the epoxy matrix. It has shown a good synergistic effect of both the particles [10]. Huang et al. [12] prepared h-BN/GO hybrid by the electrostatic

self-assembly, and their epoxy composite performed TC of 2.23 W/mK at 40 vol% filler loading. Also, they prepared h-BN/RGO hybrids, and h-BN/RGO hybrid epoxy composites exhibited a maximum TC of 3.45 W/mK when the incorporation of h-BN/RGO filler was 26.04 vol%. The enhancement of TC described that thermal conductivity of reduced graphene oxide (RGO) is greater than GO and dispersion status of h-BN/RGO hybrid filler in the polymer matrix is more viable than dispersion of h-BN/GO hybrids, for which agglomeration and voids inside resin are minimized [13].

Many researchers reported that at a high filler loading of high-density materials like metal or ceramic, TC becomes high. However, high loading, i.e., more than 60% filler fraction, pays penalty to mechanical and other properties like viscosity and bonding strength, which create hindrance in the application of high-performance electrical chip [16]. To enable a wide range of applications including high thermal conductivity at comparable less filler loading was the target of this work. In this work, h-BN and APTES-modified h-BN were incorporated in an epoxy matrix along with GO and RGO with different weight fractions [14]. This work demonstrates a new insight to fabricate a high thermal conductive hybrid composite. The thermal and mechanical properties of each of the fabricated hybrid composites were investigated at various filler fractions and correlated with monofiller-loaded epoxy composites.

## 2 Experimental

### 2.1 Raw materials

Graphene oxide (GO) (purity ~ 99%) and reduced graphene oxide (RGO) (purity ~ 98.8%) were supplied by United Nanotech Innovation Pvt. Ltd. (Bangalore, India). The h-BN powders (255475-50G) with dimension ~ 2 μm were obtained from Sigma-Aldrich Co., Germany. The epoxy is diglycidyl ether of bisphenol-A (DGEBA), named as Araldite GY 250, and the corresponding crosslinker is tri-ethylene tetra amine (TETA), named as Aradur<sup>®</sup>HY 951 IN, supplied by M/S Huntsman international (INDIA) Pvt. Ltd. 3-amino propyl triethoxysilane (APTES) was obtained from HIMEDIA Laboratories, Mumbai, India.

### 2.2 Modification of h-BN

Surface modification of h-BN was carried out by APTES. A solution of 100 ml ethanol and 6 g of h-BN was prepared by 20 min stirring which is illustrated in Fig. 1. Then, silane (APTES) coupling agent was added to that solution considering the ratio of 100:2.4 of h-BN and silane followed by 5 h of

stirring at 60 °C. Then, the resulting suspension was filtered and washed with distilled water followed by vacuum drying for 24 h at 110 °C. To get more modified h-BN (mh-BN), the above process was followed as per discussed proportionate.

### 2.3 Preparation of hybrid composites

The h-BN/GO and h-BN/RGO–epoxy hybrid composites were fabricated using hand lay-off technique which is

summarized in Table 1. The low-temperature epoxy resins and corresponding hardener were mixed in a ratio of 10:1 with hybrid particles. The required quantities of fillers were dried in a vacuum oven for 2 h at 60 °C. Before filler mixing, the predetermined epoxy resin was kept inside a vacuum oven at 70 °C for bubble removal and viscosity reduction. Then, fillers were added and followed by hand stirring. Then, sonication was ended for 2 h by ultrasonic sonicator for proper dispersion of particles in the matrix. Then, curing

Fig. 1 Flow diagram for surface modification of h-BN

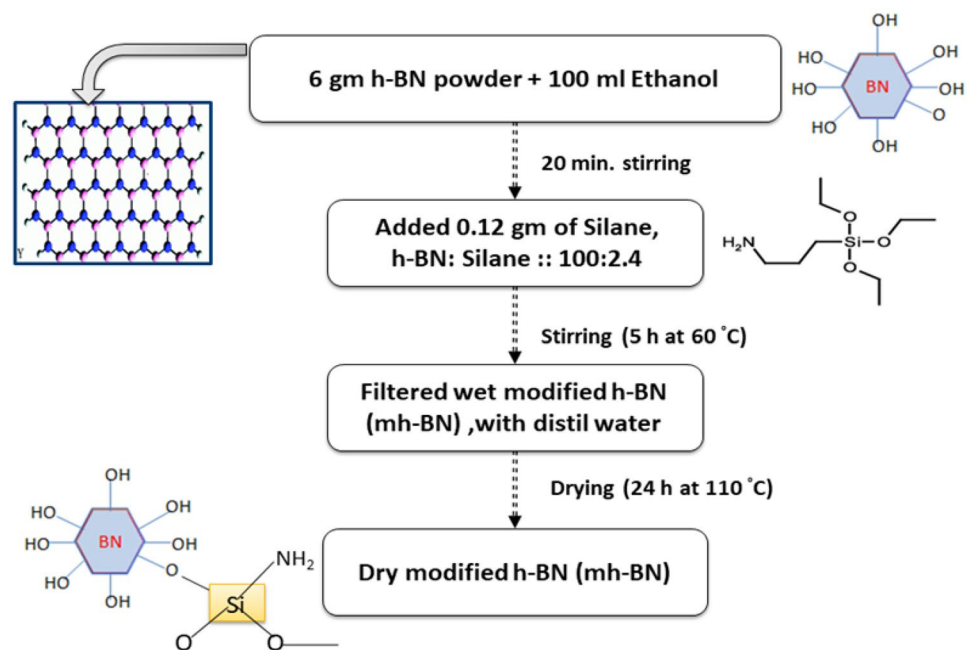


Table 1 Thermal conductivity (K, W/mK) of hybrid composites at different filler fractions

Sample name	GO/RGO filler (wt%)	h-BN/mh-BN filler (wt%)	Thermal conductivity (W/mK)	Sample name	Thermal conductivity (W/mK)
GO1/epoxy	1.5	0	0.231	RGO1/epoxy	0.242
GO2/epoxy	2.5	0	0.262	RGO2/epoxy	0.272
GO3/epoxy	3.5	0	0.312	RGO3/epoxy	0.334
GO4/epoxy	4.5	0	0.293	RGO4/epoxy	0.311
h-BN1/epoxy	0	10	0.251	mh-BN1/epoxy	0.259
h-BN2/epoxy	0	20	0.33	mh-BN2/epoxy	0.372
h-BN3/epoxy	0	30	0.44	mh-BN3/epoxy	0.48
h-BN4/epoxy	0	40	0.53	mh-BN4/epoxy	0.59
h-BN/GO1/epoxy	1.5	10	0.354	h-BN/RGO1/epoxy	0.371
h-BN/GO2/epoxy	2.5	20	0.394	h-BN/RGO2/epoxy	0.412
h-BN/GO3/epoxy	3.5	30	0.545	h-BN/RGO3/epoxy	0.603
h-BN/GO4/epoxy	4.5	40	<b>0.713</b>	h-BN/RGO4/epoxy	<b>0.789</b>
mh-BN/GO1/epoxy	1.5	10	0.381	mh-BN/RGO1/epoxy	0.484
mh-BN/GO2/epoxy	2.5	20	0.399	mh-BN/RGO2/epoxy	0.584
mh-BN/GO3/epoxy	3.5	30	0.568	mh-BN/RGO3/epoxy	0.908
mh-BN/GO4/epoxy	4.5	40	<b>0.769</b>	mh-BN/RGO4/epoxy	<b>1.416</b>

The bold indicates the optimized composition of experiment

agent was added followed by 5 min sonication. The prepared composites were poured into a mold and allowed to cure at room temperature with a load on it for 24 h. Some amounts of hybrids composites were used in the fabrication of lap shear joint specimens. The hybrid composites of different compositions were applied on mechanically polished steel substrates by carefully rubbing with 400-grade emery paper and cleaning with acetone. The uniform layer of bond line thickness (BLT) about 0.05–0.1 mm was prepared to make lap joints. As the epoxy displays high mechanical strength, it transformed to fully cured within 24 h. Following the above course of action, first GO/epoxy, RGO/epoxy composites were prepared considering wt% of 1.5, 2.5, 3.5 and 4.5 of GO and RGO separately. Then, h-BN/epoxy and mh-BN/epoxy composites were fabricated with 10, 20, 30 and 40 wt% of filler loading separately. After proper mixing of h-BN and mh-BN in an epoxy matrix, previously defined amount of GO and RGO was added followed by 3 h sonication to make hybrid composites as explained in Table 1.

## 2.4 Characterization and measurements

Laser diffraction particle size analyzer (LA-960, Horiba Scientific) was used to measure the size distribution profile or particle size of h-BN and GO water suspension in dynamic light scattering (DLS) technique. The crystalline structure of GO, RGO, h-BN and mh-BN was analyzed by X-ray diffraction (XRD) pattern from Shidzu, XRD-7000L, Japan. The source of the X-ray is CuK $\alpha$  radiation. Morphology of fillers and optimized hybrid composites was obtained by using scanning electron microscopy (SEM, EVOMA15, Carl Zeiss SMT, Germany). Fourier transform infrared (FTIR) spectroscopy (Nicolet, 6700, USA) was utilized to obtain the spectra of GO, RGO, h-BN and modified h-BN over a range 500–4000 cm<sup>-1</sup>. The thermal conductivity (K, W/mK) at 60 °C is measured on the circular sample in accordance with ASTM E 1530-06 standard by guarded heat flow meter technique (Unitherm™2022, Anterco, USA), which follows Eq. (1)

$$Q = -KA \left[ \frac{\Delta T}{\Delta x} \right] \quad (1)$$

where  $Q$  is the heat supplied (Joules/s or Watts);  $K$  is the thermal conductivity of composite (W/mK);  $A$  is the area of the sample (m<sup>2</sup>);  $\Delta x$  is the thickness of the sample (m).

The lap shear strength of four optimized hybrid composites according to standard ASTM D1002 through the universal testing machine (UTM, Instron 3382, UK) was carried out at room temperature following the pulling rate of 0.05 inch/min. The flexural strength (UTM, Instron 3382, UK) and impact strength (IT 504 Plastic impact, 899 (notch cutter) Tinius Olsen, USA) of the samples are conducted by following the standard ASTM D790 and ASTM D256,

respectively. Thermal stability of fillers and hybrid composites was carried out by a thermogravimetric analyzer (TGA, TA Instruments, USA) using indium as the reference material according to ASTM E1868. The TGA analysis was carried out by taking the sample in the pan (5–10 mg), and the temperature was increased by 10 °C/min over a temperature range 30–800 °C under nitrogen purging with a flow rate of 60 ml/min. Atomic force microscopy (AFM, XE-100, Park—South Korea) was used to observe the surface topography/morphology of optimized samples.

## 3 Results and discussion

### 3.1 Particle size

H-BN is two-dimensional white solid materials having mass density 2.29 g/cm<sup>3</sup>. The particle size distribution of h-BN is shown in Fig. 2a. DLS technique shows that the particle size of h-BN is 2.12  $\mu$ m which is defined by the manufacturer. GO is a layered structure having an average of 3–6 number of layers and bulk density of 0.4 g/cm<sup>3</sup>. Due to the presence of hydroxyl, carboxyl and carbonyl groups, GO becomes hydrophilic by nature. So it can disperse in water very well. From particle size analyzer, it is clear that as shown in Fig. 2b the mean lateral dimension of GO is 10.51  $\mu$ m.

### 3.2 X-ray diffraction analysis and SEM

Figure 3a explains the XRD patterns of GO and RGO provided by the supplier. The GO exhibits a sharp diffraction peak (001) at a diffraction angle  $2\theta = 11.5^\circ$  while in reduced GO, (001) peak disappears and a new peak (002) was observed at  $2\theta = 26.3^\circ$ . An abundant amount of functional group on the surface of GO has been removed during chemical treatment to obtain RGO. The change in peak intensity between GO and RGO is only because of the presence and absence of the oxygen-containing functional group inside the graphene layer. This may be attributed that when the interlayer space increases, the intensity of peak increases and vice versa which is also distinguishing between GO and RGO [11, 13]. As per Sreekanth Perumbilavil et al., XRD diffraction peak for pristine graphite is at  $2\theta = 26.36^\circ$  with interlayer spacing ( $d$ ) of 0.335 nm, whereas GO diffraction peak is at  $2\theta = 10.01^\circ$ . But the ' $d$ ' of GO increased to 0.854 nm due to the introduction of oxygen-containing functional groups at the time of oxidation. In the case of RGO, a new peak for  $2\theta = 32^\circ$  with  $d = 0.373$  nm signifies the exclusion of the majority of functional groups. The low intensity of RGO in Fig. 3a indicates the few-layer structure with less interplanar spacing between monolayers [35].

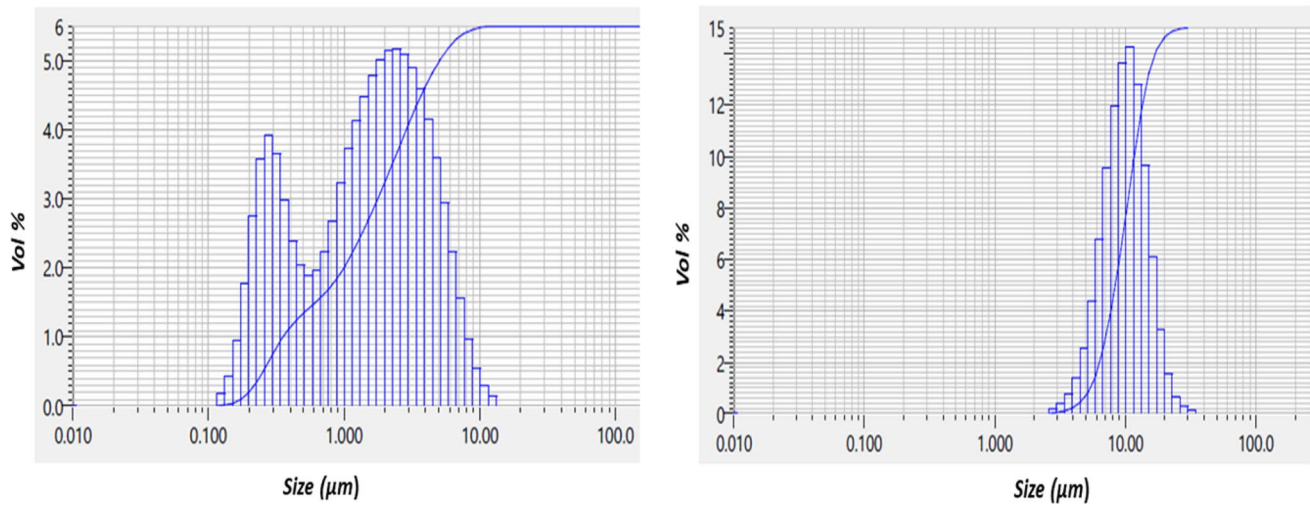


**Fig. 2** **a** DLD results of h-BN and **b** GO water suspension

**Fig. 3** **a** XRD patterns of GO and RGO, **b** SEM images of GO (i) and RGO (ii)

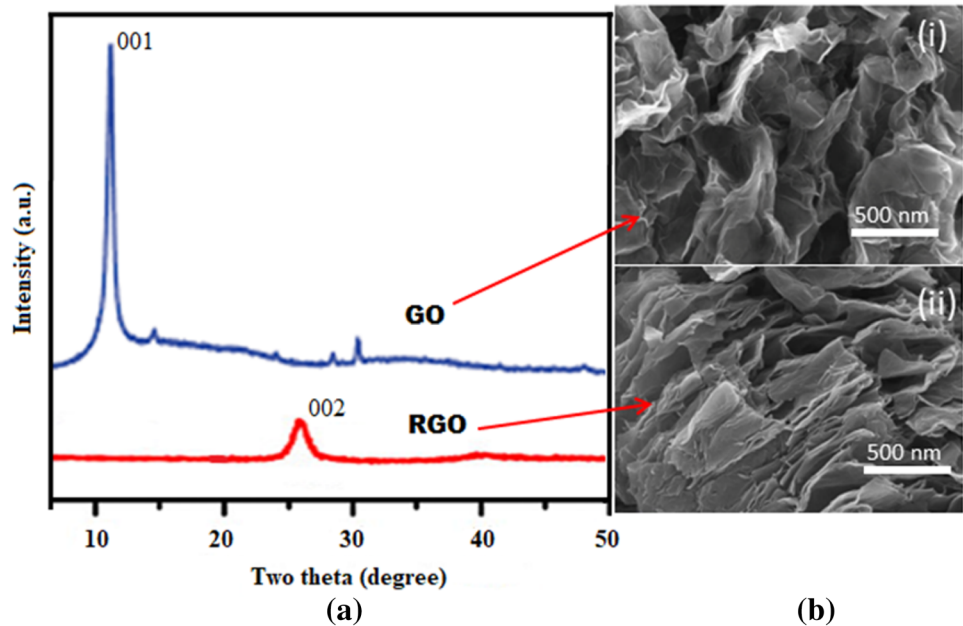


Figure 3b shows the SEM images of GO and RGO. SEM of GO [Fig. 3b(i)] shows an obvious curly layer structure with some aggregation of GO. The SEM image of RGO [Fig. 3b(ii)] appears as different layers of comparable thin sheets randomly aggregated, with distinct edges, wrinkled surfaces and folding.

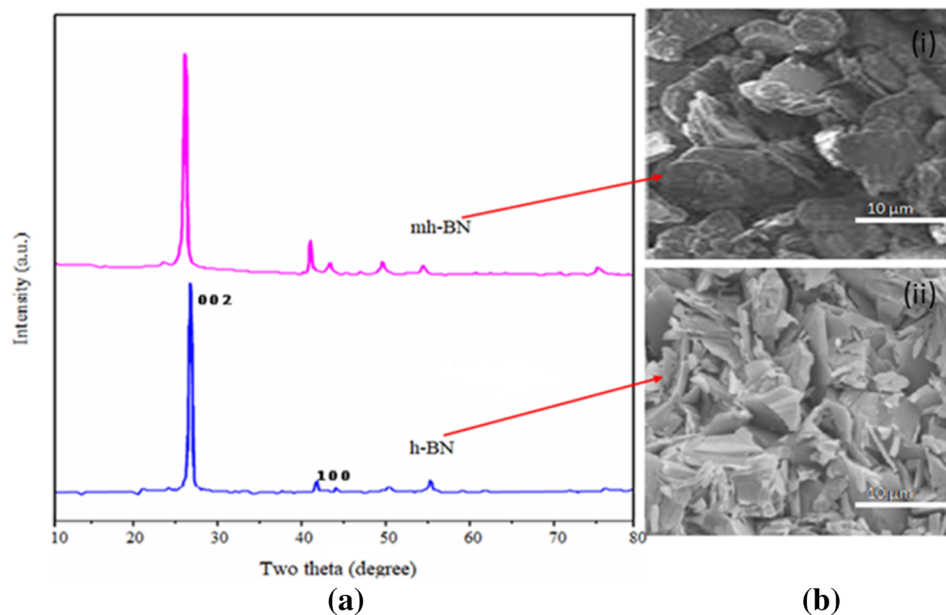
XRD patterns of h-BN and mh-BN are illustrated in Fig. 4a. All the peaks of h-BN are reliable with the standard (JCPDS: 34-0421) h-BN peaks. As there was no new peak appeared after the modification of h-BN (mh-BN), it seems that the crystal structure of h-BN particles did not change. For the pristine h-BN, the peak (002) at around  $2\theta = 26.4^\circ$  and the peak (100) at around  $2\theta = 41.9^\circ$  are observed.

Figure 4b displays the SEM image of the modified h-BN (i) and pristine h-BN (ii). From the particle size analysis and the SEM micrograph, Query it is obvious that the pristine h-BN has an average lateral size of  $2 \mu\text{m}$  which also exhibits a fine flaked structure and even surface.

### 3.3 FTIR analysis

FTIR spectra of pristine h-BN and APTES-modified h-BN are shown in Fig. 5a. It is observed that the FTIR range of pristine h-BN just exhibits a couple of assimilation peaks. h-BN displays two strong attributes in-plane B–N extending vibration at  $1393.61 \text{ cm}^{-1}$  and out-plane

**Fig. 4** **a** XRD patterns of h-BN and modified h-BN (mh-BN), **b** SEM images of mh-BN (i) and h-BN (ii)



twisting vibration at  $789.76\text{ cm}^{-1}$ . After the modification of h-BN, the few minor ingestion peaks show up close to  $2973\text{ cm}^{-1}$ , which represents the C–H extending vibrations of the hydrocarbon chain of the addition of APTES [20–22]. From Fig. 5b, GO sample shows a broad and outstanding absorption peak at  $3534\text{ cm}^{-1}$ , which can be attributed to the stretching vibration of –OH group. The stretching vibration of C=O from carbonyl and carboxylic is found at  $1744\text{ cm}^{-1}$  and C=C vibration of unoxidized graphite peak at  $1627.5\text{ cm}^{-1}$ . The peak at  $1392\text{ cm}^{-1}$  represents =C–H vibration in GO. The extra bands at  $1209\text{ cm}^{-1}$  represent C=O=C stretching vibration absorption [8, 10]. The absence of a  $3534\text{ cm}^{-1}$  peak in RGO reveals the absence

of OH group after reduction. The absorption peak at  $1601\text{ cm}^{-1}$  belongs to C=C, while the peak at  $1118\text{ cm}^{-1}$  attributed to vibration of C–OH group. These above results indicate that the elimination of partial functional groups in GO is done effectively by reduction [13, 23].

### 3.4 Thermal conductivity

Figure 6a displays the TC of GO/epoxy and RGO/epoxy composites with different filler fractions starting from 1.5 to 4.5 wt%. The maximum TC of both GO/epoxy and RGO/epoxy composites is reported at 3.5 wt% of GO and RGO which are 0.312 and 0.334 W/mK, respectively, and

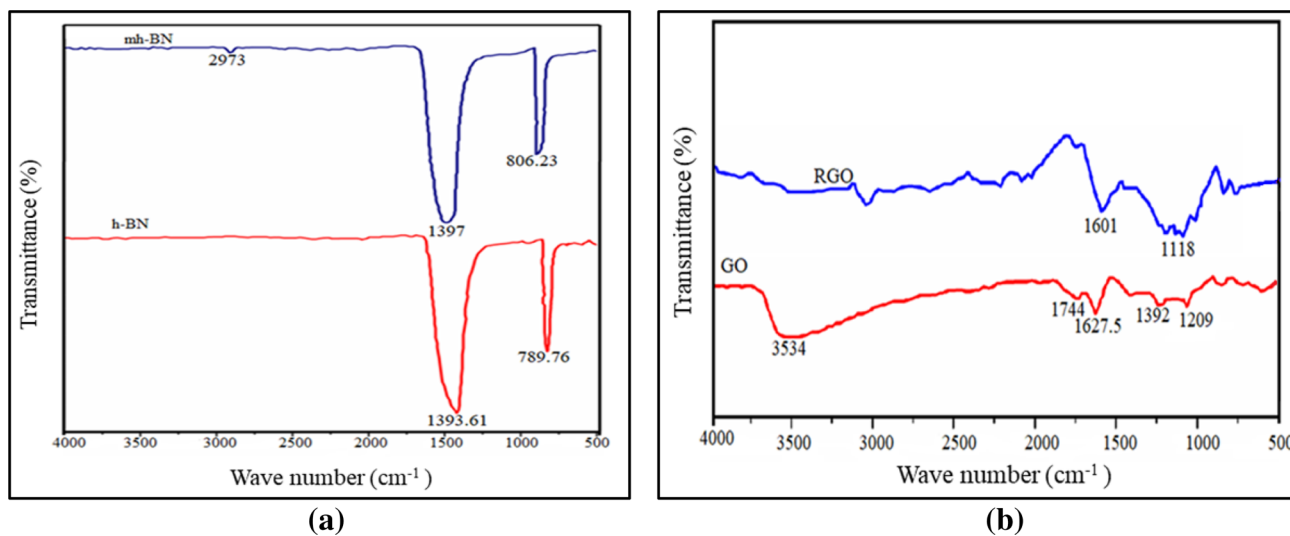


**Fig. 5** FTIR spectra of h-BN and mh-BN (a) and GO and RGO (b)

proved that RGO has higher intrinsic TC than that of GO. It was also due to the dispersion ability of RGO as filler in the epoxy matrix to minimize the agglomeration and voids [17]. But at 4.5 wt% of both GO and RGO loadings, the TC slightly decreases to 0.293 and 0.311 W/mK, respectively. This is may be due to the agglomeration and clusters formation at high filler fraction. This is quite similar to Tao Huang et al. They have demonstrated the TC value of 0.39 W/mK at 2 wt% of GO, but at 3 wt% of GO loading the TC decreased. In another work of Tao Huang, RGO shows better TC value inside epoxy [12, 13]. Also, Aradhana et al. [36] explained that the improvement in TC values up to the

certain extent of GO and RGO filler loading and TC value decreases due to agglomeration of filler. APTES-modified h-BN epoxy composite shows better results than native h-BN epoxy composite at each weight fraction described in Fig. 6b. At 40 wt% loading of h-BN and mh-BN with epoxy, the TC values were observed at 0.53 and 0.59 W/mK, respectively. This is in accordance with the Junei Gu et al. They have experimented at 40 wt% loading of both h-BN and mh-BN with epoxy, the TC value of both composites was 0.55 W/mK [2]. Also, Huang et al. [13] demonstrated that at 26.04 vol% of h-BN loading the composite showed TC value approximately 0.8 W/mK. Figure 6c

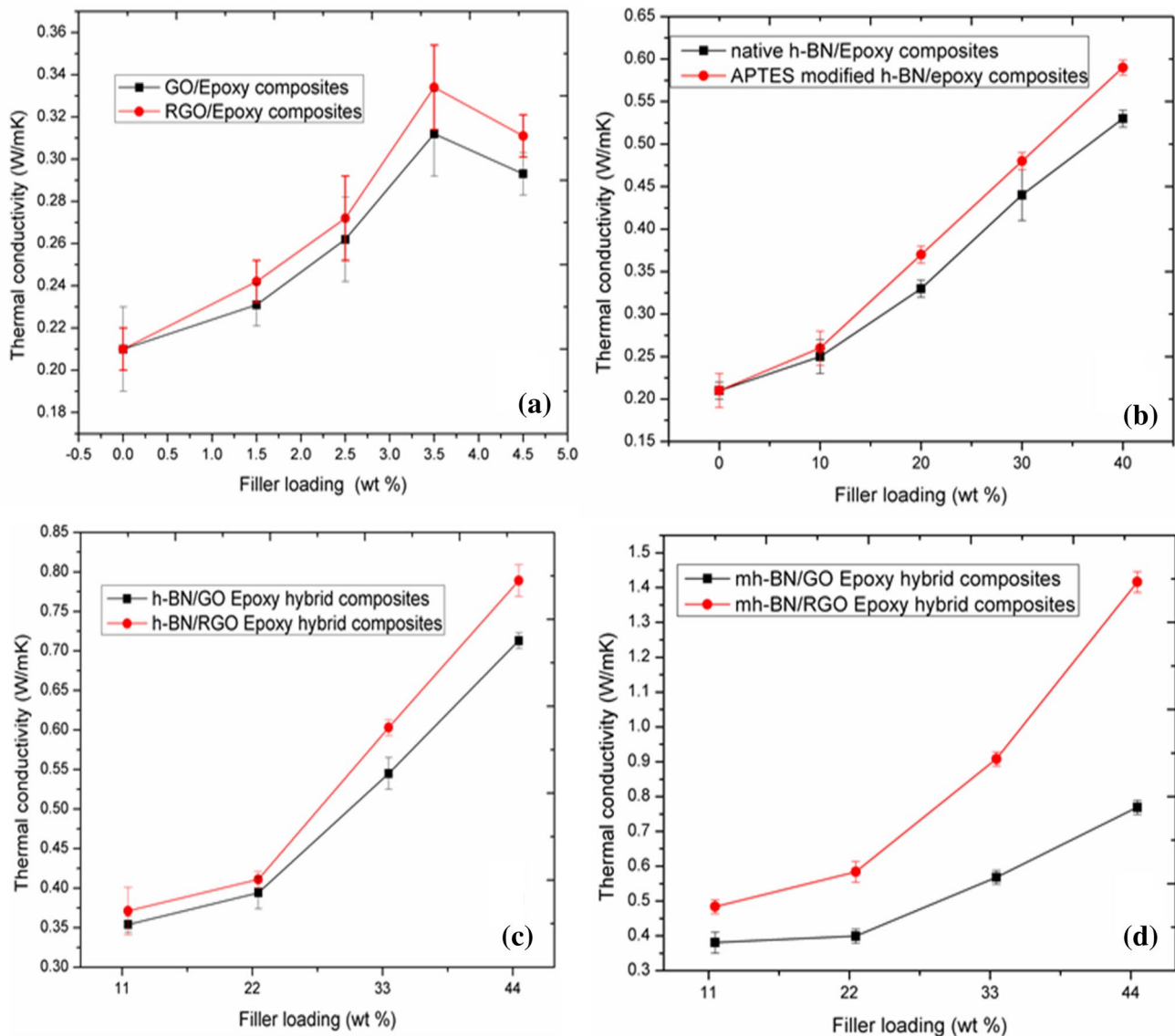


**Fig. 6** **a** Thermal conductivity of GO and RGO–epoxy composites with different filler fractions. **b** Thermal conductivity of h-BN and mh-BN–epoxy composites with different filler fractions. **c** Thermal conductivity of h-BN/GO and h-BN/RGO–epoxy hybrid composites

with different filler fractions. **d** The thermal conductivity of mh-BN/GO and mh-BN/RGO–epoxy composites with different filler fractions

describes the addition of h-BN at 10 wt% to 40 wt% with the 1.5 wt% to 4.5 wt% of GO and RGO making hybrid filler inside the epoxy matrix. Table 1 shows that the thermal conductivity values of these hybrid filler composite systems were increased as compared to single filler loading. This is because of the formation of long-range 3D conducting networks for phonon transfers inside the filler–matrix system and effect of h-BN on TC of hybrid composites, as the synergistic effect of h-BN with GO and RGO was quite appreciable. Low TC attributed to the formation of less effective three-dimensional percolation paths [18]. This is in accordance with Rajesh Kumar et al. They described that the effect of 30 wt% of h-BN on 30 wt% graphite powder is so synergistic and that the TC reached to 2.02 W/mK [18]. Effect of 10 wt% BN with 5 wt% graphene on the epoxy is described by A. K. Singh et al. They demonstrated the TC value at this loading was 1.6 W/mK [37]. The effect of modified h-BN (mh-BN) on the thermal conductivity of the hybrid composites system is shown in Fig. 6d. The TC of hybrid composites increases at the loading of mh-BN instead of h-BN with GO and RGO as defined earlier. The TC is 1.416 W/mK with 44.5 (4.5 RGO + 40 mh-BN) wt% loading of hybrid filler. After the modification of h-BN, the dispersion of h-BN inside the epoxy matrix improves. Chen et al. [38] also reported that the modified h-BN with graphene nanosheets with a mass ratio of 6:4 (total 10 wt%) with epoxy give raises the TC value of 0.48 W/mK. As per Yuan et al. [10], for the hybrid of 50 wt% of a 5-µm AlN particle with 6 wt% of GO hybrid filler, the TC of epoxy composite enhanced to 2.27 W/mK. Therefore, the interfacial phonon scattering and thermal resistance inside the epoxy are reduced efficiently. It was also cited that due to the iso-structure of h-BN and RGO, the compatibility between two hybrid particles enhances [18, 19].

### 3.5 Analytical models

The discussed experimental values of TC of different hybrid epoxy composites are examined by different simple analytical models such as Maxwell equations, model developed by Hashin–Shtrikmann for lower bound values and series model or the inverse rule of mixture equation for lower bound results. The analytical results of composite related to GO are shown in Table 2 and shown in Fig. 7 along with previously gathered experimental values [39–41].

(a)

$$\text{Maxwell equation : } \frac{K}{K_c} = 1 + 3 \left( \frac{K_d - K_c}{K_d + 2K_c} \right) \Phi \quad (2)$$

where  $K$  is the TC of the composite.  $K_d$  and  $K_c$  are the thermal conductivities of the dispersed phase (filler) and the continuous phase (matrix), respectively.

$\Phi$  represents the volume fraction of the dispersed phase.

(b)

Hashin - Shtrikman model:  $K_C$

$$= K_m \left[ \frac{2(1 - f)K_m + (1 + 2f)K_f}{(2 + f)K_m + (1 - f)K_f} \right] \quad (3)$$

where  $K_C$  is the TC of the composite.  $K_f$  and  $K_m$  are the thermal conductivities of filler and matrix, respectively. The term  $f$  represents the volume fraction of filler.

(c)

$$\text{Inverse rule of mixture/series model: } \frac{1}{K_C} = \frac{1 - f}{K_m} + \frac{f}{K_f} \quad (4)$$

Equation 4 is derived from the rule of the mixture and does not consider voids.

All the terms in Eq. 4 can be assumed as terms in Eq. 3.

Comparing the experimental TC values with calculated analytical values, it is observed that the series model estimates the lower value of TC in relation to the experimental value. In Fig. 7a, b, Maxwell and Hashin–Shtrikmann model estimates nearer to the TC values. As Hashin–Shtrikmann model is suitable for more than two filler analysis, it gives higher results of TC shown in Fig. 7c, d. From this, it is assumed that some voids and particle agglomeration have reduced the TC values of composites. However, we have

**Table 2** Thermal conductivity values from the analytical model

Sample code	Thermal conductivity (W/mK)			
	Experimental	Maxwell	Hashin–Shtrikmann	Series
Neat epoxy	0.21	0.21	0.21	0.21
GO1/epoxy	0.231	0.228	0.23	0.212
GO2/epoxy	0.262	0.256	0.258	0.243
GO3/epoxy	0.312	0.292	0.291	0.271
GO4/epoxy	0.293	0.322	0.323	0.294
h-BN1/epoxy	0.251	0.24	0.25	0.24
h-BN2/epoxy	0.33	0.31	0.299	0.29
h-BN3/epoxy	0.44	0.38	0.39	0.37
h-BN4/epoxy	0.53	0.473	0.48	0.46
h-BN/GO1/epoxy	0.354	0.348	0.344	0.338
h-BN/GO2/epoxy	0.394	0.41	0.445	0.371
h-BN/GO3/epoxy	0.545	0.532	0.583	0.491
h-BN/GO4/epoxy	<b>0.713</b>	0.681	0.728	0.643
mh-BN/GO1/epoxy	0.381	0.36	0.42	0.322
mh-BN/GO2/epoxy	0.399	0.42	0.46	0.354
mh-BN/GO3/epoxy	0.568	0.54	0.586	0.482
mh-BN/GO4/epoxy	<b>0.769</b>	0.748	0.85	0.722

The bold indicates the optimized composition of experiment



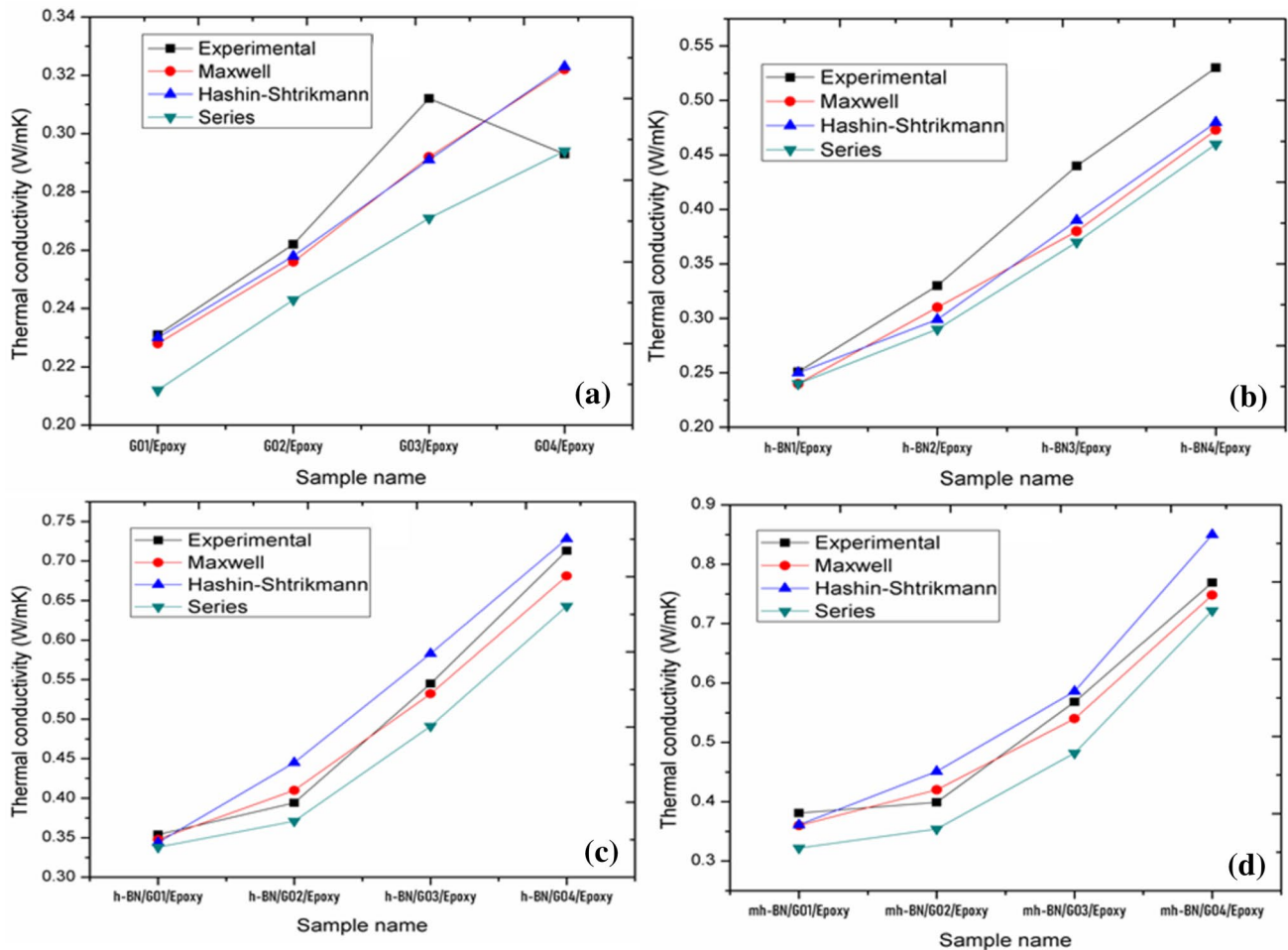


Fig. 7 Thermal conductivity enhancement comparisons with theoretical models **a** GO composites, **b** h-BN composites, **c** h-BN/GO hybrid composites, **d** mh-BN/GO hybrid composites

ignored different effective parameters such as TC ratios of fillers, size of filler and void, for these models to calculate the values. From Fig. 7, it is proved that TC is increasing with the increase in filler addition and also the effect of hybrid filler contributes to the TC enhancement [40, 41].

### 3.6 Lap shear strength

Figure 8 illustrates the lap shear strength of four different cured hybrid composites entitled as h-BN/GO4/epoxy, h-BN/RGO4/epoxy, mh-BN/GO4/epoxy and mh-BN/RGO4/epoxy with respect to lap shear strength value of neat epoxy. These tests were conducted considering the single lap shear joint of stainless steel plate as substrates. Out of different surface preparation methods, mechanical polishing was adopted for creating strong and durable adhesive–substrate bond strength. The mechanical polishing of steel plate substrate establishes oxygen-deficient iron oxide ( $Fe_2O_3$ ) on the surface for better joint strength

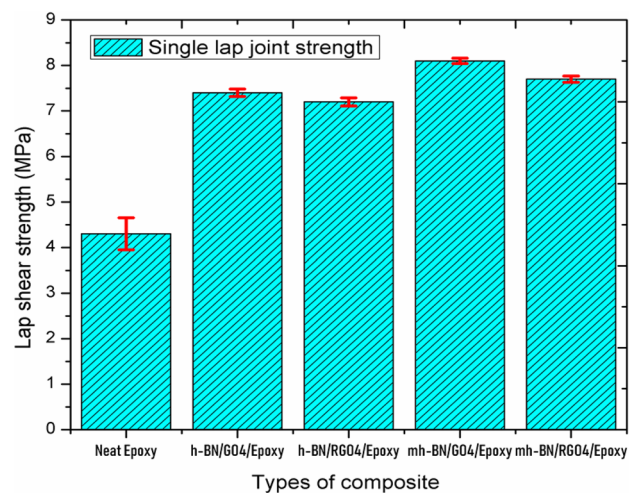


Fig. 8 Single lap shear strength of different optimized compositions

(Fig. 9(3)). So, the reaction between epoxy composites as adhesive and substrate is improved due to electron sharing with the oxygen present in epoxide dimer and trimer, for which high joint strength is formed between substrate and epoxy composites as adhesives. The reported results were the average of three measurements considering standard deviation [24, 25].

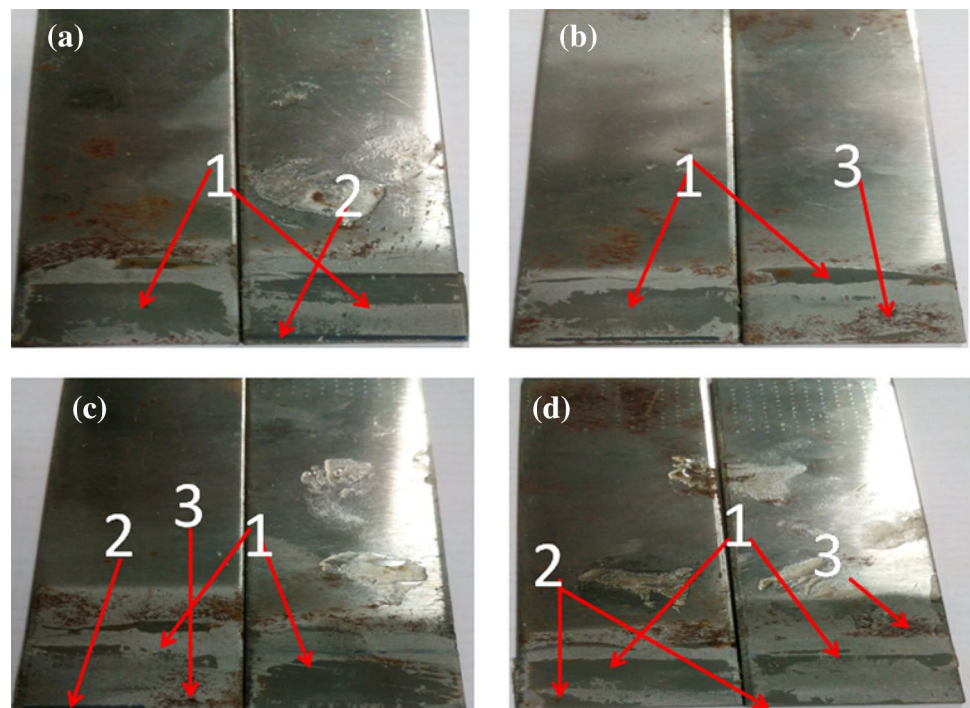
From Fig. 8, the composites termed as h-BN/GO4/epoxy and h-BN/RGO4/epoxy are the hybrid composite of GO and RGO with unmodified h-BN with optimal filler loading. In Fig. 8, it is observed that h-BN/GO4/epoxy hybrid composite shows better lap shear strength of 7.4 MPa which is slightly better than h-BN/RGO4/epoxy hybrid composite. This may be due to the presence of more functional groups like hydroxyl group in GO which could set up the high joint strength between the substrate and hybrid composites than RGO. The composites titled as mh-BN/GO4/epoxy and mh-BN/RGO4/epoxy represent the optimized hybrid filler loading of GO and RGO with modified h-BN. As the modified h-BN has the ability for better dispersion within the matrix, the tensile strength has increased, and consequently, mh-BN/GO4/epoxy hybrid composite showed improved lap shear strength of 8.1 MPa with respect to mh-BN/RGO4/epoxy hybrid composite with lap shear strength of 7.6 MPa. This was also due to the compatibility of GO and mh-BN as they are iso-structure and having more number of functional groups which can bind filler with matrix effectively and hybrid composites with substrate [18].

Lap shear strength properties of an adhesive joint are the function of bond line thickness (BLT) of adhesive and surface modification of the substrate, which affects the interfacial bond strength and cohesive strength of adhesives. The enhancement of adhesive joint strength with the hybrid filler content may be due to the resistance to fracture contributed by the hybrid fillers with the help of crack blunting mechanism. Different types of failure/fracture are shown in Fig. 9. The presence of both cohesive and interfacial failures on the joint area of lap predicts the propagation of cracks through the bulk of composites and then shifts to an interface which required more energy to create failure [24, 26].

### 3.7 Flexural and impact strength

Figure 10 shows the plots of flexural (Fig. 10a) and impact strength (Fig. 10b) for four different optimized compositions of GO/RGO/h-BN/mh-BN/epoxy hybrid composites along with neat epoxy. All the optimized hybrid composites carry the filler loading of 44.5 wt% (40 wt% h-BN/mh-BN + 4.5 wt% GO/RGO). The flexural strength and impact strength of neat epoxy are 131 MPa and 13 kJ/m<sup>2</sup>, respectively. Then flexural and impact strength of hybrid composites named as h-BN/GO4/epoxy and h-BN/RGO4/epoxy decrease dramatically with respect to neat epoxy and made a small enhancement when modified h-BN (mh-BN) is loaded into the epoxy instead of pristine h-BN represented as mh-BN/GO4/epoxy and mh-BN/RGO4/epoxy. This is due to the better distribution of mh-BN as

**Fig. 9** Fracture surface of single lap shear joint of **a** h-BN/GO4/epoxy, **b** h-BN/RGO4/epoxy, **c** mh-BN/GO4/epoxy and **d** mh-BN/RGO4/epoxy hybrid composites showing different types of failure process: (1) interfacial failure, (2) cohesive failure and (3) formation of iron oxide



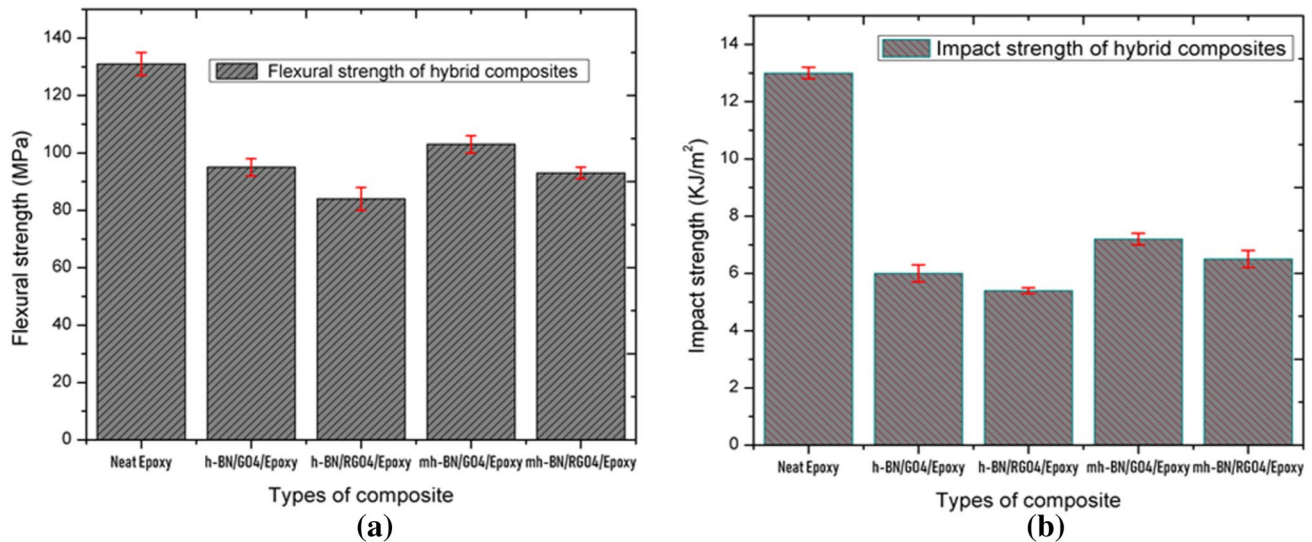


Fig. 10 Flexural strength (a) and impact strength (b) of different optimized hybrid composites

compared to pristine h-BN. With the extreme addition of hybrid filler to the epoxy matrix, an incomplete dispersion of hybrid filler takes place and the formation of the voids and stress concentration points occurs for which mechanical properties of hybrid composites decrease with respect to neat epoxy [2, 28, 29]. From Fig. 10a, b, it is also observed that matrix carrying GO with h-BN and GO with mh-BN has little higher properties than corresponding RGO with h-BN and RGO with mh-BN. This is due to that GO layers have disrupted  $sp^2$  structure carrying various functional groups which can react with epoxy and harden and toughen the interfacial bond strength of composites. They also have lateral flexibility with a high aspect ratio which can improve the flexural strength of composites if reinforced [27]. But RGO cannot transfer its mechanical strength as aromatic rings restore. So, the recovery  $sp^2$  type structure establishes more  $\pi$ - $\pi$  interactions for which restacking of RGO layers occurs. This creates an impact on the surface area and wettability of reinforcement [30, 31].

### 3.8 Thermogravimetric analysis (TGA)

The TGA curve of neat epoxy and the four optimized hybrid composites is illustrated in Fig. 11. The thermal decomposition temperature for neat epoxy is 355.73 °C, whereas hybrid composites known as (1) h-BN/GO4/epoxy, (2) h-BN/RGO4/epoxy, (3) mh-BN/GO4/epoxy, (4) mh-BN/RGO4/epoxy are showing the thermal decomposition temperature of 376.71, 378.84, 372.82 and 374.53 °C, respectively. From the resulted data, it is comprehensible that the four hybrid composites are showing better results than neat epoxy. It is primarily due to the efficient combination of hybrid particles with epoxy. Moreover, h-BN with GO

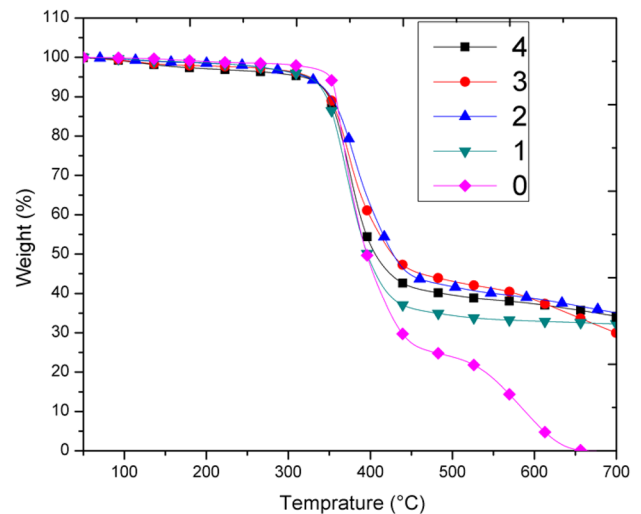


Fig. 11 TGA curves of (0) neat epoxy (1) h-BN/GO4/epoxy, (2) h-BN/RGO4/epoxy, (3) mh-BN/GO4/epoxy (4) mh-BN/RGO4/epoxy

and RGO has good compatibility in an epoxy matrix, which restricts the movement of the polymer chain for easy decomposition. So, the hybrid fillers absorb the thermal energy, resulting in the rise in decomposition temperature of hybrid composites [2, 18]. The sample exhibiting maximum thermal decomposition temperature is h-BN/RGO4/epoxy hybrid composite, which contains 40 wt% unmodified h-BN and 4.5 wt% of RGO. This is due to the thermal stability of unmodified h-BN which is better than modified h-BN (mh-BN) because in modified h-BN thermal degradation occurs due to the presence of grafted group on the surface of h-BN [32]. As compared to sample manifest as h-BN/GO4/epoxy hybrid composite, containing the

same amount of filler as sample h-BN/RGO4/epoxy hybrid composite, the only difference is GO, RGO and having less thermal decomposition temperature, i.e., 376.71 °C. This is because the thermal stability of RGO is better than GO, because of the presence of moisture and more oxygen functional groups in GO as related to RGO, which reduces the degradation temperature of GO [33, 34]. In a similar way, we can identify the reason behind the thermal decomposition temperature of sample mh-BN/GO4/epoxy hybrid composite is 372.82 °C and sample mh-BN/RGO4/epoxy hybrid composite is 374.53 °C.

### 3.9 Atomic force microscopy (AFM)

The surface topography/morphology (captured under contact mode) of hybrid composites with 2D and 3D image profile containing modified h-BN (mh-BN) and unmodified h-BN with RGO in the epoxy matrix is demonstrated in AFM image (Fig. 11). The height images in Fig. 12a, b contain the height data on the surface area of 10

by 10  $\mu\text{m}^2$ . In contact mode operation of AFM, the probe tip was brought into contact with the composite surface at a constant deflection. The image (Fig. 12a) demonstrates that there is good interfacial interaction between hybrid filler and epoxy matrix, which may be the source of good thermal and consistent mechanical properties. The surface homogeneity is quite evident in Fig. 12a. Also, the presence of these hybrid particles (mh-BN and RGO) results in surface roughness, which is in good agreement with AFM images in Fig. 12a. The agglomeration of unmodified h-BN with RGO is evidently visible in Fig. 12b, whereas mh-BN shows a good distribution with RGO in the epoxy matrix as illustrated in Fig. 12a.

### 3.10 Scanning electron microscopy (SEM)

The fracture surface or morphology of h-BN/RGO4/epoxy hybrid composite is shown in Fig. 13a, b. With the addition of 44.5 wt% of the total hybrid filler of unmodified h-BN and RGO, the fracture line has been created on the surface

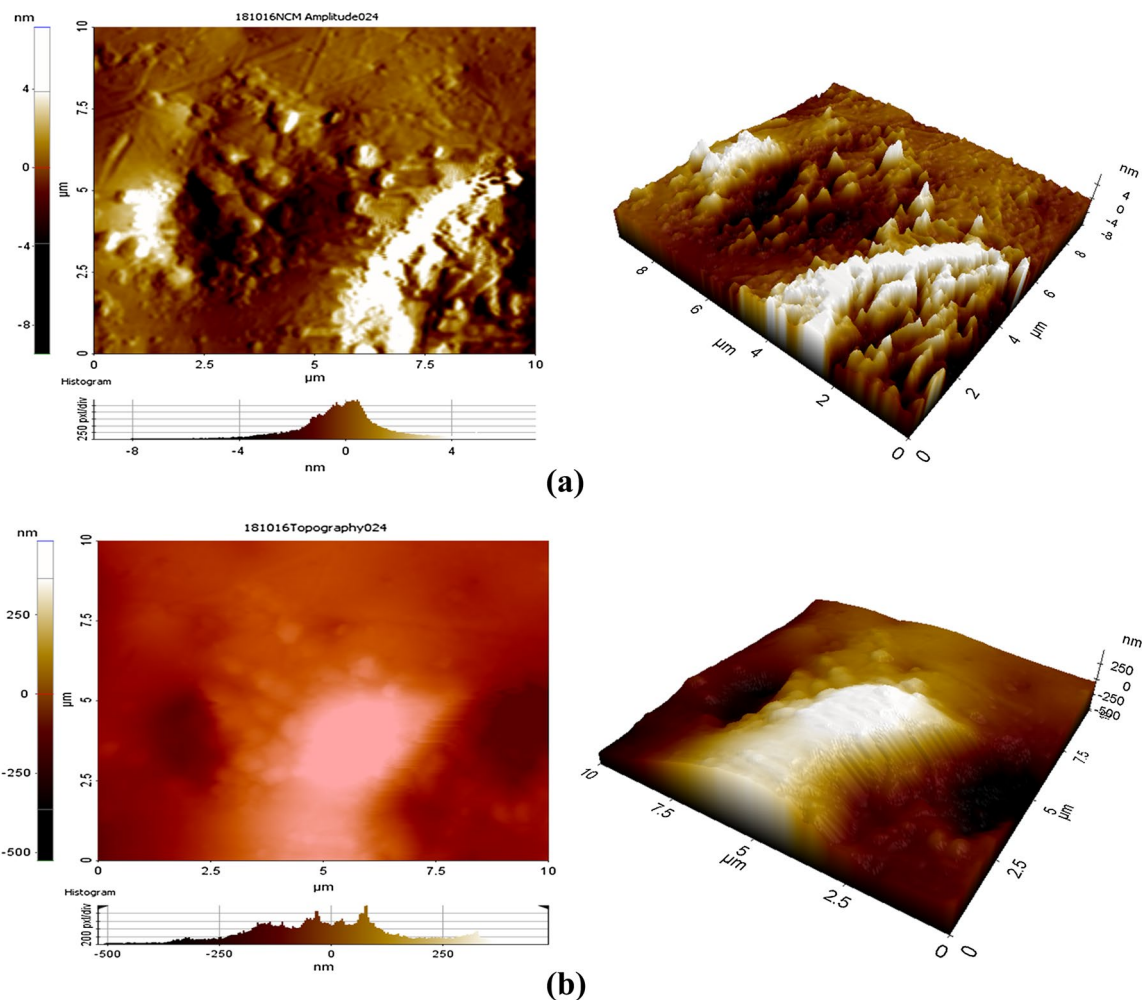


**Fig. 12** Image of atomic force microscopy for optimized hybrid composites. **a** mh-BN/RGO4/epoxy, **b** h-BN/RGO4/epoxy

marked under the white circle. The red arrows represent the void developed at the time of fabrication of composite as the result of improper dispersion of hybrid filler with the matrix as the consequence of gas bubble, defects and stress concentration point are introduced. Therefore, lap shear, flexural and impact strength of h-BN/RGO4/epoxy hybrid composites is less than mh-BN/RGO4/epoxy hybrid composite which is shown in Figs. 8 and 10. As is discussed earlier, the APTES coupling agent has the ability to improve interfacial contact between the inorganic filler and epoxy matrix. Thus, the modified h-BN displays improved dispersion inside the epoxy matrix with RGO and prevents stubborn agglomeration of the fillers, which is demonstrated in Fig. 13c, d. Irrespective of 44.5 wt% of hybrid filler loading in the mh-BN/RGO4/epoxy hybrid composite, it shows better compatibility with the epoxy matrix as illustrated in Fig. 13c, d.

## 4 Conclusion

The fabrication of thermal interface material (TIM) based on epoxy adhesive incorporating hybrid filler of GO and RGO with h-BN is purposefully done. It was found that the thermal conductivity of pristine epoxy (0.21 W/mK) enhanced gradually with the incorporation of GO or RGO with h-BN and mh-BN. The maximum value of thermal conductivity is 1.416 W/mK which is obtained due to the addition of RGO (4.5 wt%) and mh-BN (40 wt%) hybrid in an epoxy matrix. Different analytical models also approved thermal conductivity enhancement. In this study, the effect of GO and RGO with h-BN and mh-BN was illustrated from lap shear strength, flexural strength and impact strength. It was attributed that the four optimized compositions of GO, RGO, h-BN and mh-BN with epoxy show a better result with respect to high filler-loaded epoxy composites. Also, the thermal stability of all the four optimized hybrid composites performed well up to 250 °C. Thus, mh-BN/RGO4/epoxy

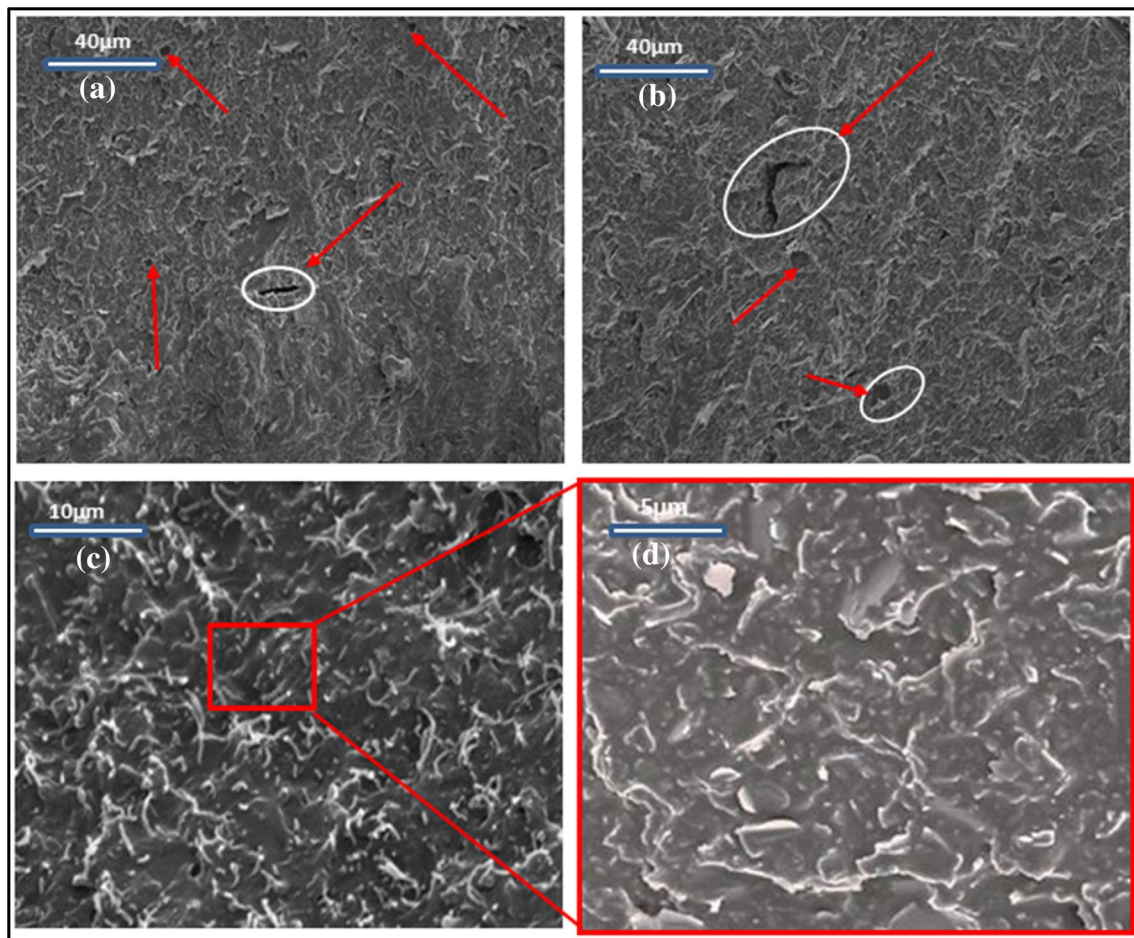


Fig. 13 SEM images of h-BN/RGO4/epoxy (a, b), mh-BN/RGO4/epoxy (c, d)

hybrid composite has the potential to use as thermal interface material (TIMs) in microelectronics packaging and thermal sensor connection.

**Acknowledgments** This work is supported by the Board of Research Board in Nuclear Science (BRNS), Department of Atomic Energy (DAE), Government of India (Project No. 39/14/01/2018-BRNS/39001).

### Compliance with ethical standards

**Conflict of interest** The authors declare that they have no conflict of interest.

**Informed consent** We declare that this work is completely original, and research was conducted of in a sound mind considering or following different articles previously published. We are giving our consent for any further clarification.

### References

- Wang Z, Fu Y, Meng W, Zhi C (2014) Solvent-free fabrication of thermally conductive insulating epoxy composites with boron nitride nanoplatelets as fillers. *Nanoscale Res Lett* 9(1):643
- Gu J, Zhang Q, Dang J, Xie C (2012) Thermal conductivity epoxy resin composites filled with boron nitride. *Polym Adv Technol* 23(6):1025–1028
- Srinivas K, Bhagyashekar MS (2015) Thermal conductivity enhancement of epoxy by hybrid particulate fillers of graphite and silicon carbide. *J Miner Mater Charact Eng* 3(02):76
- Eichler J, Lesniak C (2008) Boron nitride (BN) and BN composites for high-temperature applications. *J Eur Ceram Soc* 28(5):1105–1109
- Mahanta NK, Loos MR, Zloczower IM, Abramson AR (2015) Graphite–graphene hybrid filler system for high thermal conductivity of epoxy composites. *J Mater Res* 30(7):959–966
- An F, Li X, Min P, Li H, Dai Z, Yu ZZ (2018) Highly anisotropic graphene/boron nitride hybrid aerogels with long-range ordered architecture and moderate density for highly thermally conductive composites. *Carbon* 126:119–127
- Muthu RN, Rajashabala S, Kannan R (2016) Facile synthesis and characterization of a reduced graphene oxide/halloysite nanotubes/hexagonal boron nitride (RGO/HNT/h-BN) hybrid nanocomposite and its potential application in hydrogen storage. *RSC Adv* 6(82):79072–79084
- Yu H, Zhang B, Bulin C, Li R, Xing R (2016) High-efficient synthesis of graphene oxide based on improved hummer's method. *Sci Rep* 6:36143
- Park W, Guo Y, Li X, Hu J, Liu L, Ruan X, Chen YP (2015) High-performance thermal interface material based on few-layer graphene composite. *J Phys Chem C* 119(47):26753–26759
- Yuan W, Xiao Q, Li L, Xu T (2016) Thermal conductivity of epoxy adhesive enhanced by hybrid graphene oxide/AlN particles. *Appl Therm Eng* 106:1067–1074
- Wang Z, Qi R, Wang J, Qi S (2015) Thermal conductivity improvement of epoxy composite filled with expanded graphite. *Ceram Int* 41(10):13541–13546
- Huang T, Zeng X, Yao Y, Sun R, Meng F, Xu J, Wong C (2016) Boron nitride@ graphene oxide hybrids for epoxy composites with enhanced thermal conductivity. *RSC Adv* 6(42):35847–35854
- Huang T, Zeng X, Yao Y, Sun R, Meng F, Xu J, Wong C (2017) A novel h-BN–RGO hybrids for epoxy resin composites achieving enhanced high thermal conductivity and energy density. *RSC Adv* 7(38):23355–23362
- Mun SY, Lim HM, Lee SH (2018) Thermal and electrical properties of epoxy composite with expanded graphite-ceramic core-shell hybrids. *Mater Res Bull* 97:19–23
- Baruch AE, Bielenki L, Regev O (2012) Thermal conductivity improvement of electrically nonconducting composite materials. *Rev Chem Eng* 28(1):61–71
- Hansson J, Nilsson TM, Ye L, Liu J (2018) Novel nanostructured thermal interface materials: a review. *Int Mater Rev* 63(1):22–45
- Huang L, Zhu P, Li G, Lu DD, Sun R, Wong C (2014) Core–shell SiO<sub>2</sub>@ RGO hybrids for epoxy composites with low percolation threshold and enhanced thermo-mechanical properties. *J Mater Chem A* 2(43):18246–18255
- Kumar R, Nayak SK, Sahoo S, Panda BP, Mohanty S, Nayak SK (2018) Study on thermal conductive epoxy adhesive based on adopting hexagonal boron nitride/graphite hybrids. *J Mater Sci Mater Electron* 29(19):16932–16938
- Cui X, Ding P, Zhuang N, Shi L, Song N, Tang S (2015) Thermal conductive and mechanical properties of polymeric composites based on solution-exfoliated boron nitride and graphene nanosheets: a morphology-promoted synergistic effect. *ACS Appl Mater Interfaces* 7(34):19068–19075
- Chiang TH, Hsieh TE (2006) A study of encapsulation resin containing hexagonal boron nitride (hBN) as inorganic filler. *J Inorg Organomet Polym Mater* 16(2):175–183
- Donnay M, Tzavalas S, Logakis E (2015) Boron nitride filled epoxy with improved thermal conductivity and dielectric breakdown strength. *Compos Sci Technol* 110:152–158
- Fujihara T, Cho HB, Nakayama T, Suzuki T, Jiang W, Suematsu H, Niihara K (2012) Field-induced orientation of hexagonal boron nitride nanosheets using microscopic mold for thermal interface materials. *J Am Ceram Soc* 95(1):369–373
- Gong Y, Li D, Fu Q, Pan C (2015) Influence of graphene microstructures on electrochemical performance for supercapacitors. *Prog Nat Sci Mater Int* 25(5):379–385
- Mittal KL, Pizzi A (1999) Adhesion promotion techniques: technological applications. CRC Press, Boca Raton
- Kolb HC, Finn MG, Sharpless KB (2001) Click chemistry: diverse chemical function from a few good reactions. *Angew Chem Int Ed Engl* 40(11):2004–2021
- Ghosh PK, Halder S, Goyat MS, Karthik G (2013) Study on thermal and lap shear characteristics of epoxy adhesive loaded with metallic and non-metallic particles. *J Adhes* 89(1):55–75
- Hu K, Kulkarni DD, Choi I, Tsukruk VV (2014) Graphene-polymer nanocomposites for structural and functional applications. *Prog Polym Sci* 39(11):1934–1972
- Lee AY, Chong MH, Park M, Kim HY, Park SJ (2014) Effect of chemically reduced graphene oxide on epoxy nanocomposites for flexural behaviors. *Carbon Lett* 15(1):67–70
- Tang LC, Wan YJ, Yan D, Pei YB, Zhao L, Li YB, Lai GQ (2013) The effect of graphene dispersion on the mechanical properties of graphene/epoxy composites. *Carbon* 60:16–27
- Subhani T, Latif M, Ahmad I, Rakha SA, Ali N, Khurram AA (2015) Mechanical performance of epoxy matrix hybrid nanocomposites containing carbon nanotubes and nanodiamonds. *Mater Des* 87:436–444
- Yousefi N, Lin X, Zheng Q, Shen X, Pothnis JR, Jia J, Kim JK (2013) Simultaneous in situ reduction, self-alignment and covalent bonding in graphene oxide/epoxy composites. *Carbon* 59:406–417
- Yu Z, Wang X, Bian H, Jiao L, Wu W, Dai H (2018) Enhancement of the heat conduction performance of boron nitride/cellulosic fibre insulating composites. *PLoS ONE* 13(7):e0200842

33. Yaragalla S, Rajendran R, Jose J, AlMaadeed MA, Kalarikkal N, Thomas S (2016) Preparation and characterization of green graphene using grape seed extract for bioapplications. *Mater Sci Eng C* 65:345–353
34. Wu T, Wang X, Qiu H, Gao J, Wang W, Liu Y (2012) Graphene oxide reduced and modified by soft nanoparticles and its catalysis of the Knoevenagel condensation. *J Mater Chem* 22(11):4772–4779
35. Perumbilavil S, Sankar P, Priya Rose T, Philip R (2015) White light Z-scan measurements of ultrafast optical nonlinearity in reduced graphene oxide nanosheets in the 400–700 nm region. *Appl Phys Lett* 107(5):051104
36. Aradhana R, Mohanty S, Nayak SK (2018) Comparison of mechanical, electrical and thermal properties in graphene oxide and reduced graphene oxide filled epoxy nanocomposite adhesives. *Polymer* 141:109–123
37. Singh AK, Panda BP, Mohanty S, Nayak SK, Gupta MK (2017) Synergistic effect of hybrid graphene and boron nitride on the cure kinetics and thermal conductivity of epoxy adhesives. *Polym Adv Technol* 28(12):1851–1864
38. Chen H, Zhao C, Xu S, Yang, X (2017) Preparation and properties study of thermally conductive epoxy/modified boron nitride/graphene nanosheets composites. In: IOP conference series: materials science and engineering, vol 274, no. 1. IOP Publishing, p 012043
39. Pal R (2007) New models for thermal conductivity of particulate composites. *J Reinf Plast Compos* 26(7):643–651
40. Ngo IL, Vattikuti SP, Byon C (2017) A modified Hashin-Shtrikman model for predicting the thermal conductivity of polymer composites reinforced with randomly distributed hybrid fillers. *Int J Heat Mass Transf* 114:727–734
41. Lee JK (2007) Prediction of thermal conductivity of composites with spherical fillers by successive embedding. *Arch Appl Mech* 77(7):453–460

**Publisher's Note** Springer Nature remains neutral with regard to jurisdictional claims in published maps and institutional affiliations.